



## COPY RIGHT

**2017 IJIEMR.** Personal use of this material is permitted. Permission from IJIEMR must be obtained for all other uses, in any current or future media, including reprinting/republishing this material for advertising or promotional purposes, creating new collective works, for resale or redistribution to servers or lists, or reuse of any copyrighted component of this work in other works. No Reprint should be done to this paper, all copy right is authenticated to Paper Authors

IJIEMR Transactions, online available on 24<sup>th</sup> July 2017. Link :

<http://www.ijiemr.org/downloads.php?vol=Volume-6&issue=ISSUE-5>

Title: PV Cell Fed Step-Up Resonant Converter for Induction Motor Drive Application.

Volume 06, Issue 05, Page No: 2081 – 2088.

Paper Authors

\* **K. SAI SURESH , Sri. P. LAKSHMI NARAYANA.**

\* Dept of EEE, QIS College of Engineering & Technology.



USE THIS BARCODE TO ACCESS YOUR ONLINE PAPER

To Secure Your Paper As Per **UGC Guidelines** We Are Providing A Electronic Bar Code



## PV CELL FED STEP-UP RESONANT CONVERTER FOR INDUCTION MOTOR DRIVE APPLICATION

\*K. SAI SURESH, \*\*Sri. P. LAKSHMI NARAYANA

\*PG Scholar, Dept of EEE, QIS College of Engineering & Technology, Ongole, A.P, India,

\*\*Associate Professor, Dept of EEE, QIS College of Engineering & Technology, Ongole, A.P, India.

### ABSTRACT

In the hybrid micro grid, processes of multiple dc-ac dc or ac-dc-ac conversions are reduced in an individual ac or dc grid. The hybrid grid consists of both ac and dc networks connected together by multi directional converters. In this micro grid network, it is especially difficult to support the critical load without incessant power supply. The generated power can be extracted under varying wind speed, solar irradiation level and can be stored in batteries at low power demands. In this paper, a hybrid AC-DC micro grid with solar energy, energy storage, and a pulse load is proposed. This micro grid can be viewed as a PEV parking garage power system or a ship's power system that utilizes sustainable energy and is influenced by a pulse load. The battery banks inject or absorb energy on the DC bus to regulate the DC side voltage. The frequency and voltage of the AC side are regulated by a bidirectional AC-DC inverter. The power flow control of these devices serves to increase the system's stability and robustness. The system is simulated in Matlab/Simulink.

**Index Terms** :Renewable energy, resonant converter, soft switching, voltage step-up, voltage stress.

### I. INTRODUCTION

In general, manufacturers provide 5 second and ½ an hour surge figures which give an indication of how much power is supplied by the inverter. Solar inverters require a high efficiency rating. Since use of solar cells remains relatively costly, it is paramount to adopt high efficiency inverter to optimize the performance of solar energy system. High reliability helps keep maintenance cost low. Since most solar power stations are built in rural areas without any monitoring manpower, it requires that inverters have competent circuit structure, strict selection of components and protective functions such as internal short circuit protection, overheating protection and overcharge protection. Wider tolerance to DC input current plays an important role, since the terminal voltage varies depending on the load and sunlight [1-4]. Though energy storage batteries are significant in providing consistent power supply, variation in voltage increases as the battery's remaining capacity and internal

resistance condition changes especially when the battery is ageing, widening its terminal voltage variation range. In mid-to-large capacity solar energy systems, inverters' power output should be in the form of sine waves which attain less distortion in energy transmission. Many solar energy power stations are equipped with gadgets that require higher quality of electricity grid which, when connected to the solar systems, requires sine waves to avoid electric harmonic pollution from the public power supply.[5] How Inverters Work: There are three major functions an inverter provides to ensure the operation of a solar system One of the most efficient and promising way to solve this problem is the use of pumping and water treatment systems supplied by photovoltaic (PV) solar energy. Such systems aren't new, and are already used for more than three decades [6-8].

But until recently the majority of the available commercial converters are based on an intermediate storage system performed with the

use of batteries or DC motors to drive the water pump. The batteries allow the system to always operate at its rated power even in temporary conditions of low solar radiation [9-10]. This facilitates the coupling of the electric dynamics of the solar panel and the motor used for pumping. Generally, batteries used in this type of system have a low life span, only two years on average, which is extremely low compared to useful life of 15 years of a photovoltaic module. Also, they make the cost of installation and maintenance of such systems substantially high. Furthermore, the lack of batteries replacement is responsible for total failure of such systems in isolated areas this type of system normally uses low-voltage DC motors, thus avoiding a boost stage between the PV module and the motor [11].

Unfortunately, DC motors have low efficiency and high maintenance cost and are not suitable. For such applications the use of a three phase induction motor, due to its high degree of robustness, low cost, higher efficiency and lower maintenance cost compared to other types of motors. These requirements make necessary use of a converter with features high efficiency; low cost; autonomous operation; robustness and high life span [12-13].

## II. CONVERTER STRUCTURE AND OPERATION PRINCIPLE

The proposed resonant step-up converter is shown in Fig. 1.

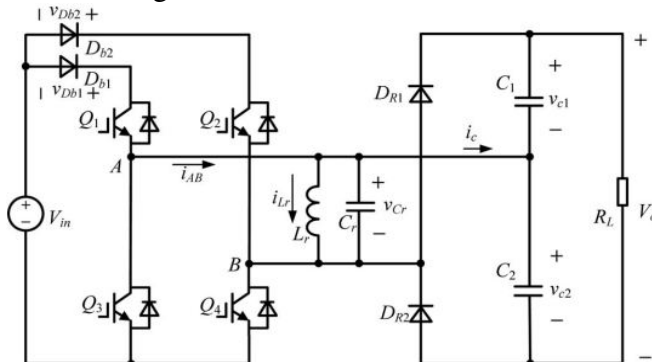


Fig. 1. Topology of the proposed resonant step-up converter.

The converter is composed of an FB switch network, which comprises Q1 through Q4, an LC parallel resonant tank, a voltage doubler rectifier, and two input blocking diodes, Db1 and Db2.

The steady-state operating waveforms are shown in Fig. 2 and detailed operation modes of the proposed converter are shown in Fig. 3. For the proposed converter, Q2 and Q3 are tuned on and off simultaneously; Q1 and Q4 are tuned on and off simultaneously. In order to simplify the analysis of the converter, the following assumptions are made:

- 1) all switches, diodes, inductor, and capacitor are ideal components;
- 2) output filter capacitors C1 and C2 are equal and large enough so that the output voltage  $V_o$  is considered constant in a switching period  $T_s$ .

### A. Mode 1 [ $t_0, t_1$ ] [See Fig. 3(a)]

During this mode, Q1 and Q4 are turned on resulting in the positive input voltage  $V_{in}$  across the LC parallel resonant tank, i.e.,  $v_{Lr} = v_{Cr} = V_{in}$ . The converter operates similar to a conventional boost converter and the resonant inductor  $L_r$  acts as the boost inductor with the current through it increasing linearly from  $I_0$ . The load is powered by C1 and C2. At  $t_1$ , the resonant inductor current  $i_{Lr}$  reaches  $I_1$

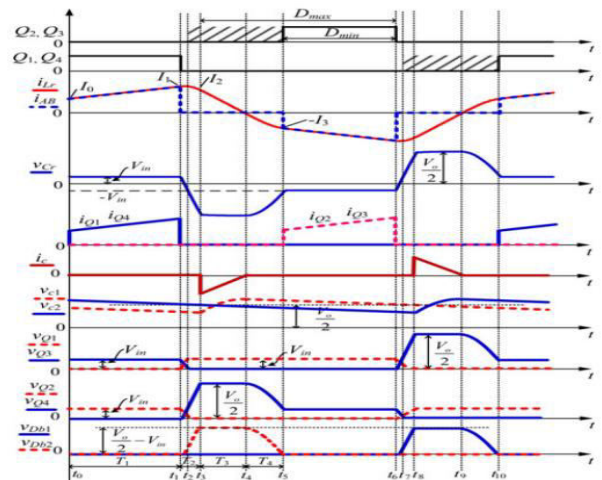


Fig. 2. Operating waveforms of the proposed converter.



$$I_1 = I_0 + \frac{V_{in}T_1}{L_r} \quad (1)$$

Where T1 is the time interval of t0 to t1.

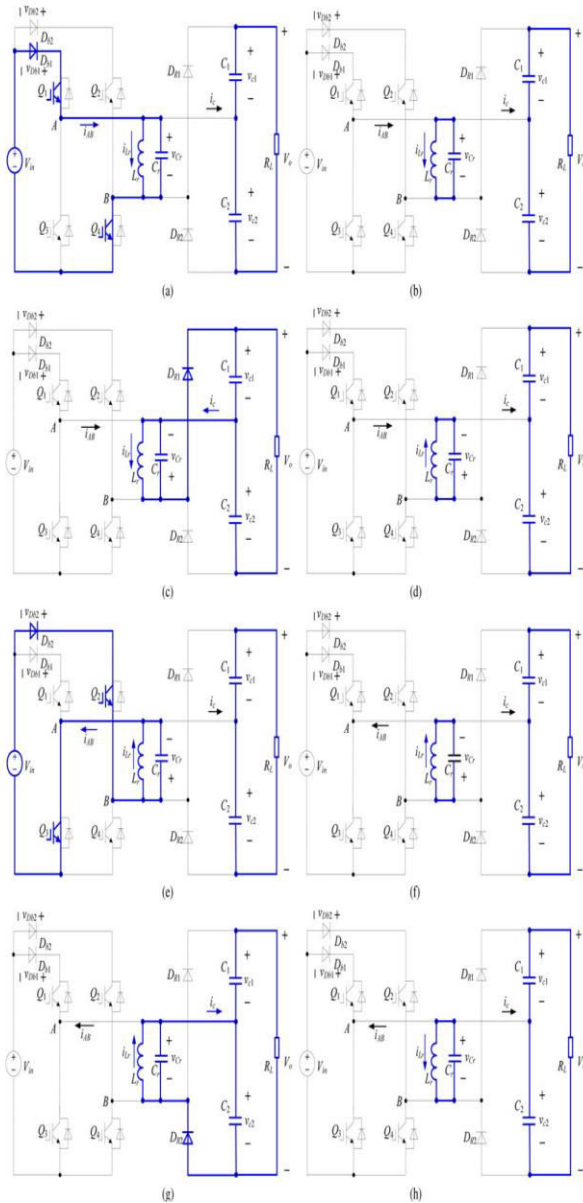


Fig. 3. Equivalent circuits of each operation stages. (a) [t0, t1]. (b) [t1, t3]. (c) [t3, t4]. (d) [t4, t5]. (e) [t5, t6]. (f) [t6, t8]. (g) [t8, t9]. (h) [t9, t10].

In this mode, the energy delivered from Vin to Lr is

$$E_{in} = \frac{1}{2}L_r (I_1^2 - I_0^2) \quad (2)$$

## B. Mode 2 [t1, t3] [See Fig. 3(b)]

At t1, Q1 and Q4 are turned off and after that Lr resonates with Cr, vCr decreases from Vin, and iLr increases from I1 in resonant form. Taking into account the parasitic output

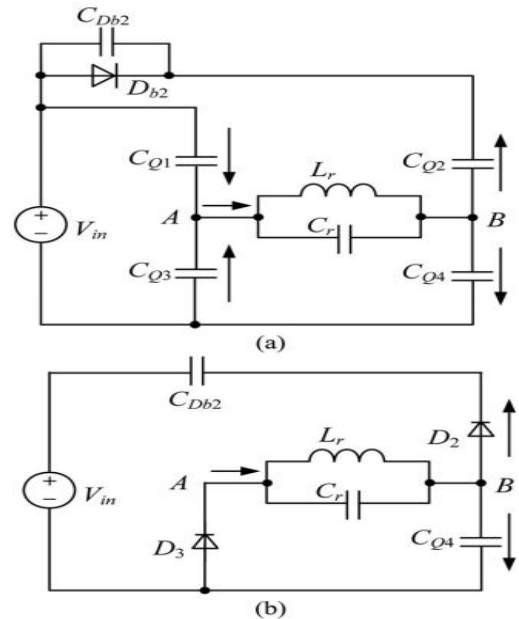


Fig. 4. Further equivalent circuits of Mode 2. (a) [t1, t2]. (b) [t2, t3].

capacitors of Q1 through Q4 and junction capacitor of Db2, the equivalent circuit of the converter after t1 is shown in Fig. 4(a), in which CDb2, CQ1, and CQ4 are charged, CQ2 and CQ3 are discharged. In order to realize zero-voltage switching (ZVS) for Q2 and Q3, an additional capacitor, whose magnitude is about ten times with respect to CQ2, is connected in parallel with Db2. Hence, the voltage across Db2 is considered unchanged during the charging/discharging process and Db2 is equivalent to be shorted. Due to Cr is much larger than the parasitic capacitances, the voltages across Q1 and Q4 increase slowly. As a result, Q1 and Q4 are turned off at almost zero voltage in this mode. When vCr drops to zero, iLr reaches its maximum magnitude. After that, vCr increases in negative direction and iLr declines in resonant form. At t2, vCr =

$-V_{in}$ , the voltages across Q1 and Q4 reach  $V_{in}$ , the voltages across Q2 and Q3 fall to zero and the two switches can be turned on under zero-voltage condition. It should be noted that although Q2 and Q3 could be turned on after  $t_2$ , there are no currents flowing through them. After  $t_2$ ,  $L_r$  continues to resonate with  $C_r$ ,  $v_{Cr}$  increases in negative direction from  $-V_{in}$ ,  $i_{Lr}$  declines in resonant form.  $D_{b2}$  will hold reversed-bias voltage and the voltage across Q4 continues to increase from  $V_{in}$ . The voltage across Q1 is kept at  $V_{in}$ . The equivalent circuit of the converter after  $t_2$  is shown in Fig. 4(b), in which D2 and D3 are the antiparallel diodes of Q2 and Q3, respectively. This mode runs until  $v_{Cr}$  increases to  $-V_o/2$  and  $i_{Lr}$  reduces to  $I_2$ , at  $t_3$ , the voltage across Q4 reaches  $V_o/2$  and the voltage across  $D_{b2}$  reaches  $V_o/2 - V_{in}$ . It can be seen that during  $t_1$  to  $t_3$ , no power is transferred from the input source or to the load, and the whole energy stored in the LC resonant tank is unchanged, i.e.,

$$\frac{1}{2}L_r I_1^2 + \frac{1}{2}C_r V_{in}^2 = \frac{1}{2}L_r I_2^2 + \frac{1}{2}C_r \left(\frac{V_o}{2}\right)^2 \quad (3)$$

We have

$$i_{Lr}(t) = \frac{V_{in}}{Z_r} \sin[\omega_r(t - t_1)] + I_1 \cos[\omega_r(t - t_1)] \quad (4)$$

$$V_{Cr}(t) = V_{in} \cos[\omega_r(t - t_1)] - I_1 Z_r \sin[\omega_r(t - t_1)] \quad (5)$$

$$T_2 = \frac{1}{\omega_r} \left[ \arcsin \left( \frac{V_{in}}{\sqrt{V_{in}^2 + \frac{L_r I_1^2}{C_r}}} \right) + \arcsin \left( \frac{V_o}{2\sqrt{V_{in}^2 + \frac{L_r I_1^2}{C_r}}} \right) \right] \quad (6)$$

Where  $\omega_r = 1/\sqrt{L_r C_r}$ ,  $Z_r = L_r/C_r$ , and  $T_2$  is the time interval of  $t_1$  to  $t_3$ .

### C. Mode 3 [ $t_3, t_4$ ] [See Fig. 3(c)]

At  $t_3$ ,  $v_{Cr} = -V_o/2$ , DR1 conducts naturally, C1 is charged by  $i_{Lr}$  through DR1,  $v_{Cr}$  keeps

unchanged, and  $i_{Lr}$  decreases linearly. At  $t_4$ ,  $i_{Lr} = 0$ . The time interval of  $t_3$  to  $t_4$  is

$$T_3 = \frac{2I_2 L_r}{V_o} \quad (7)$$

The energy delivered to load side in this mode is

$$E_{out} = \frac{V_o I_2 T_3}{4} \quad (8)$$

The energy consumed by the load in half-switching period is

$$E_R = \frac{V_o I_o T_s}{2} \quad (9)$$

Assuming 100% conversion efficiency of the converter and according to the energy conservation rule, in half-switching period

$$E_{in} = E_{out} = E_R \quad (10)$$

Combining (7), (8), (9), and (10), we have

$$I_2 = V_o \sqrt{\frac{I_o T_s}{V_o L_r}} \quad (11)$$

$$T_3 = 2 \sqrt{\frac{I_o T_s L_r}{V_o}} \quad (12)$$

### D. Mode 4 [ $t_4, t_5$ ] [See Fig. 3(d)]

At  $t_4$ ,  $i_{Lr}$  decreases to zero and the current flowing through DR1 also decreases to zero, and DR1 is turned off with zero current switching (ZCS); therefore, there is no reverse recovery. After  $t_4$ ,  $L_r$  resonates with  $C_r$ ,  $C_r$  is discharged through  $L_r$ ,  $v_{Cr}$  increases from  $-V_o/2$  in positive direction, and  $i_{Lr}$  increases from zero in negative direction. Meanwhile, the voltage across Q4 declines from  $V_o/2$ . At  $t_5$ ,  $v_{Cr} = -V_{in}$ , and  $i_{Lr} = -I_3$ . In this mode, the whole energy stored in the LC resonant tank is unchanged, i.e., where  $T_4$  is the time interval of  $t_4$  to  $t_5$ .

$$\frac{1}{2}C_r \left(\frac{V_o}{2}\right)^2 = \frac{1}{2}L_r I_3^2 + \frac{1}{2}C_r V_{in}^2 \quad (13)$$

We have

$$I_o = I_3 = \frac{1}{2} \sqrt{\frac{C_r (V_o^2 - 4V_{in}^2)}{L_r}} \quad (14)$$

$$i_{Lr}(t) = -\frac{V_o}{2\omega_r L_r} \sin[\omega_r(t - t_5)] \quad (15)$$

$$v_{Cr}(t) = \frac{-V_o \cos[\omega_r(t - t_5)]}{2} \quad (16)$$

$$T_4 = \frac{1}{\omega_r} \arccos\left(\frac{2V_{in}}{V_o}\right) \quad (17)$$

### E. Mode 5 [t5, t6] [See Fig. 3(e)]

If Q2 and Q3 are turned on before t5, then after t5, Lr is charged by Vin through Q2 and Q3, iLr increases in negative direction, and the mode is similar to Mode 1. If Q2 and Q3 are not turned on before t5, then after t5, Lr will resonate with Cr, the voltage of node A vA will increase from zero and the voltage of node B vB will decay from Vin; zero-voltage condition will be lost if Q2 and Q3 are turned on at the moment. Therefore, Q2 and Q3 must be turned on before t5 to reduce switching loss. The operation modes during [t6, t10] are similar to Modes 2–4, and the detailed equivalent circuits are shown in Fig. 3(f)–(h). During [t6, t10], Q2 and Q3 are turned off at almost zero voltage, Q1 and Q4 are turned on with ZVS, and DR2 is turned off with ZCS.

## III. MATLAB/SIMULATION RESULTS

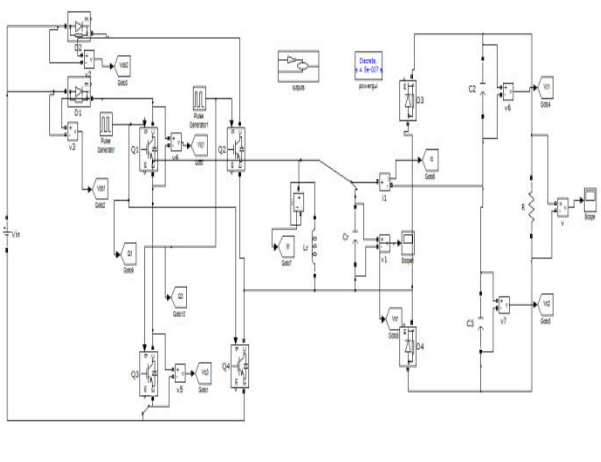


Fig.5. Matlab circuit for Resonant Boost converter

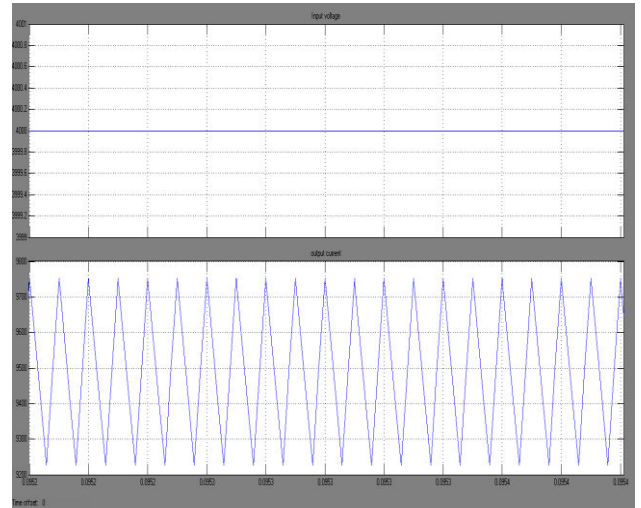


Fig.6. Simulation waveform of resonant boost converter Input voltage and Output current

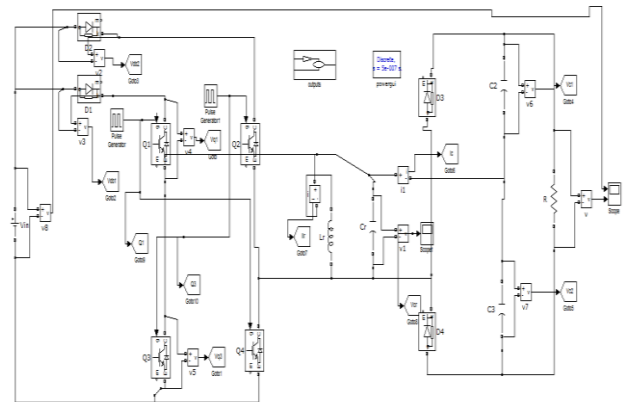


Fig.7. Matlab circuit Proposed resonant step-up converter under steady state condition

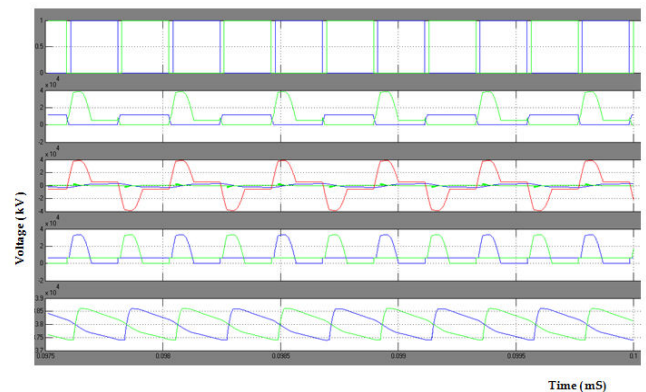
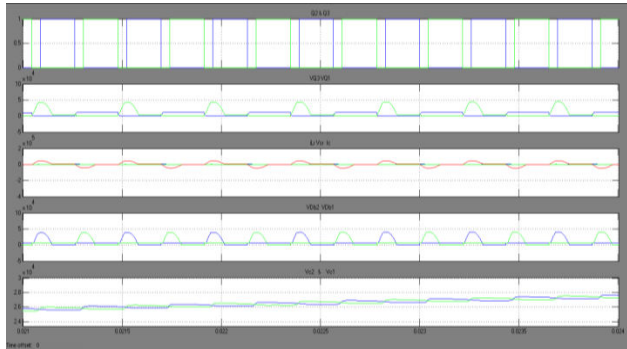


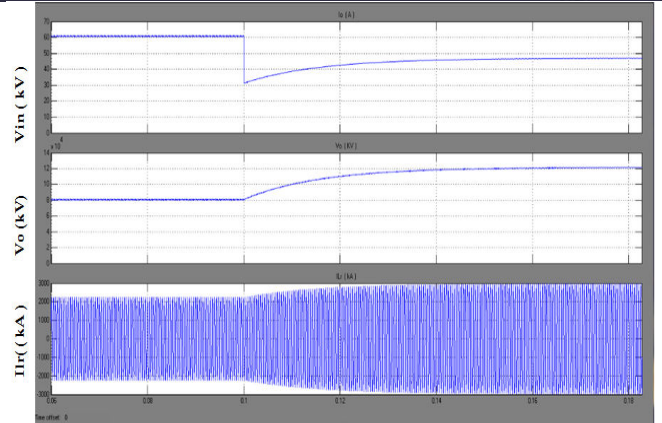
Fig.8. Steady state simulation at Vin = 4kV at 5MW load





(b)

Fig.8. Simulation circuit of Steady-state simulation results under different load conditions when  $V_{in} = 4$  kV. (a) 5 MW. (b) 1 MW.



(b)

Fig.10. Dynamic simulation results (a) Input voltage step. (b) Load step.

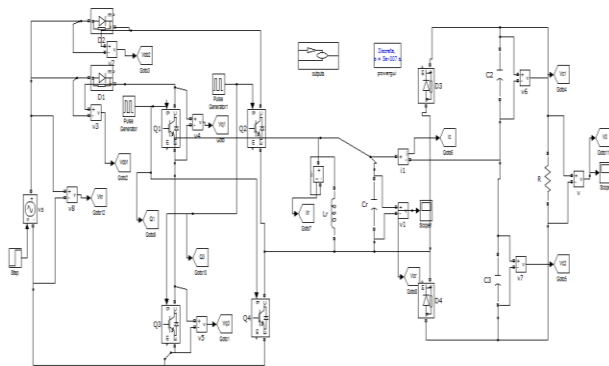
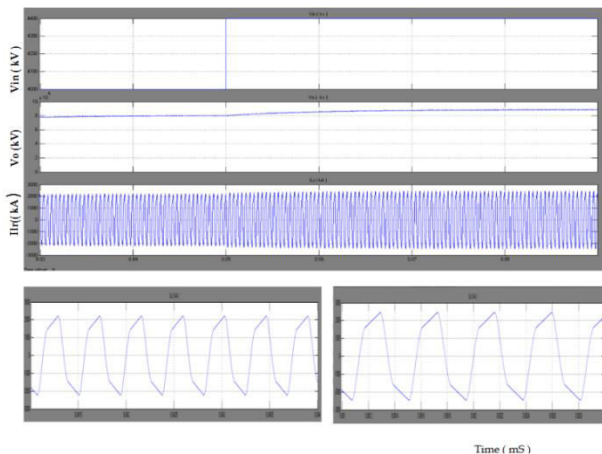


Fig.9. Matlab circuit Proposed resonant step-up converter under dynamic state condition



(a)

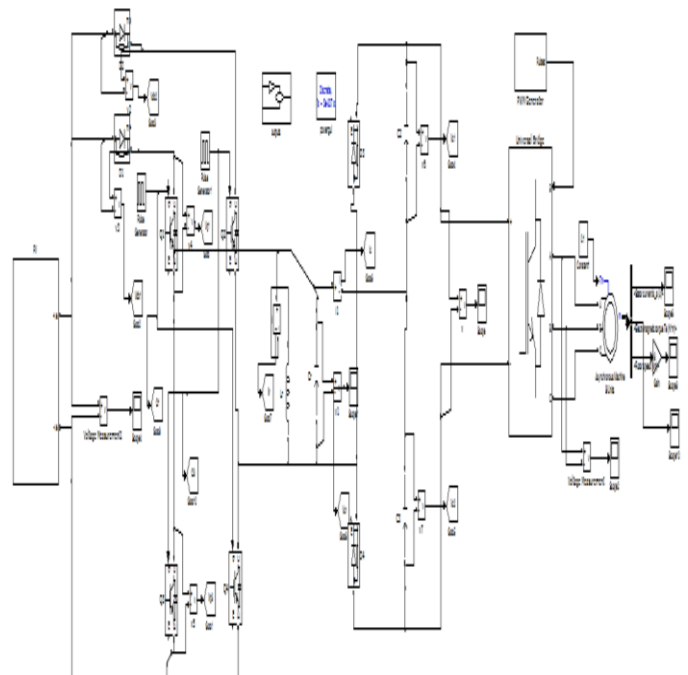


Fig.11. Matlab circuit for step up converter connected with Induction motor Drive

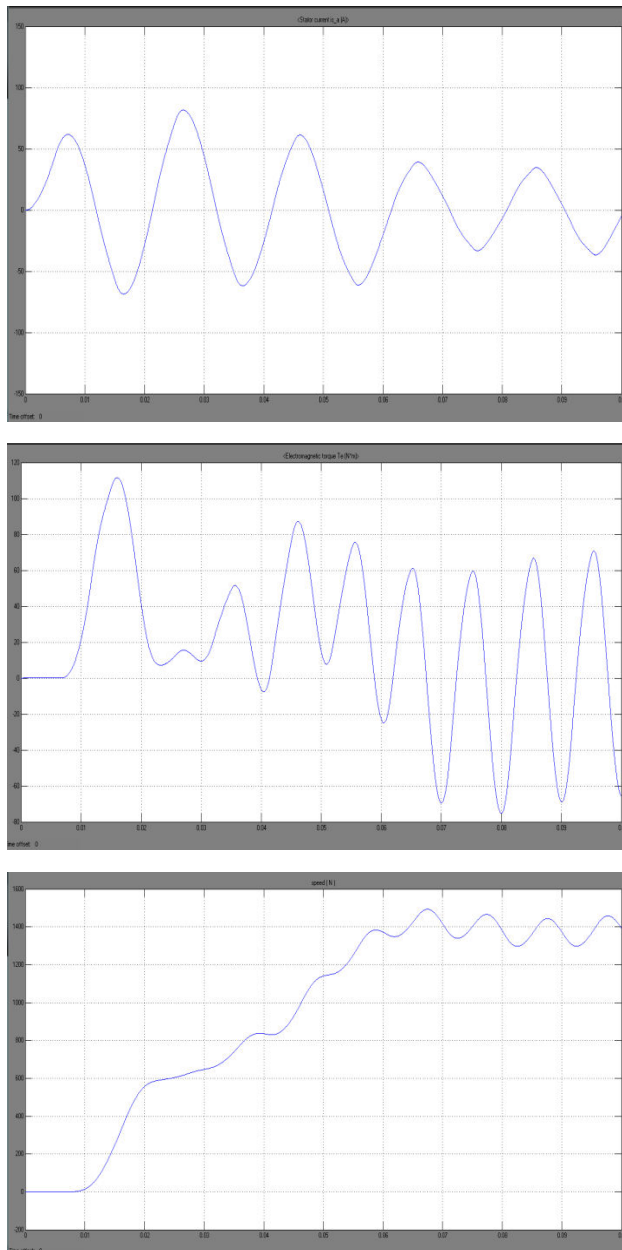


Fig.12. Speed, Stator current and Torque

## IV.CONCLUSIONS

A novel resonant dc–dc converter is proposed in this paper, which can achieve very high step-up voltage gain and it is suitable for high-power high-voltage applications. The converter utilizes the resonant inductor to deliver power by charging from the input and discharging at the output. The resonant capacitor is employed

to achieve zero-voltage turn-on and turn-off for the active switches and ZCS for the rectifier diodes. In this paper, the converter was designed to drive a three phase induction motor directly from PV solar energy and was conceived to be a commercially viable high efficiency, and high robustness.

## REFERENCES

- [1]. Wu Chen, Member, IEEE, Xiaogang Wu, Liangzhong Yao, Senior Member, IEEE, Wei Jiang, Member, IEEE, and Renjie Hu "A Step-up Resonant Converter for Grid-Connected Renewable Energy Sources" IEEE Transactions On Power Electronics, Vol. 30, No. 6, June 2015.
- [2] CIGRE B4-52 Working Group, HVDC Grid Feasibility Study. Melbourne, Vic., Australia: Int. Council Large Electr. Syst., 2011.
- [3] A. S. Abdel-Khalik, A. M. Massoud, A. A. Elserougi, and S. Ahmed, "Optimum power transmission-based droop control design for multi-terminal HVDC of offshore wind farms," IEEE Trans. Power Syst., vol. 28, no. 3, pp. 3401–3409, Aug. 2013.
- [4] F. Deng and Z. Chen, "Design of protective inductors for HVDC transmission line within DC grid offshore wind farms," IEEE Trans. Power Del., vol. 28, no. 1, pp. 75–83, Jan. 2013.
- [5] F. Deng and Z. Chen, "Operation and control of a DC-grid offshore wind farm under DC transmission system faults," IEEE Trans. Power Del., vol. 28, no. 1, pp. 1356–1363, Jul. 2013.
- [6] C. Meyer, "Key components for future offshore DC grids," Ph.D. dissertation, RWTH Aachen Univ., Aachen, Germany, pp. 9–12, 2007.



[7] W. Chen, A. Huang, S. Lukic, J. Svensson, J. Li, and Z. Wang, "A comparison of medium voltage high power DC/DC converters with high step-up conversion ratio for offshore wind energy systems," in Proc. IEEE Energy Convers. Congr.Expo., 2011, pp. 584–589.

[8] L. Max, "Design and control of a DC collection grid for a wind farm," Ph.D. dissertation, Chalmers Univ. Technol., Goteborg, Sweden, pp. 15–30, 2009.

[9] Y. Zhou, D. Macpherson, W. Blewitt, and D. Jovicic, "Comparison of DCDC converter topologies for offshore wind-farm application," in Proc. Int. Conf. Power Electron. Mach. Drives, 2012, pp. 1–6.

[10] S. Fan, W. Ma, T. C. Lim, and B. W. Williams, "Design and control of a wind energy conversion system based on a resonant dc/dc converter," IET Renew. Power Gener., vol. 7, no. 3, pp. 265–274, 2013.

[11] F. Deng and Z. Chen, "Control of improved full-bridge three-level DC/DC converter for wind turbines in a DC grid," IEEE Trans. Power Electron., vol. 28, no. 1, pp. 314–324, Jan. 2013.

[12] C. Meyer, M. Hoing, A. Peterson, and R. W. De Doncker, "Control and design of DC grids for offshore wind farms," IEEE Trans. Ind. Appl., vol. 43, no. 6, pp. 1475–1482, Nov./Dec. 2007.

[13] C. Meyer and R. W. De Doncker, "Design of a three-phase series resonant converter for offshore DC grids," in Proc. IEEE Ind. Appl. Soc. Conf., 2007, pp. 216–223.

## **Author's Profile:**

**Kunchala Sai Suresh** is doing M.Tech degree in Power Electronics & Power Systems at QIS College of Engineering & Technology (Autonomous) under JNTU, Kakinada. In 2017. At present, he is engaged in "PV Cell fed Step-up Resonant Converter for Induction Motor Drive Application".

**Sri.P. LakshmiNarayana** presently working as associate professor of the EEE department in Qis College Engineering & Technology, Ongole, A.P, India.